





Article

Modification of Biocorrosion and Cellular Response of Magnesium Alloy WE43 by Multiaxial Deformation

Natalia Anisimova ^{1,2} , Natalia Martynenko ³, Keryam Novruzov ¹, Olga Rybalchenko ³ , Mikhail Kiselevskiy ^{1,2}, Georgy Rybalchenko ⁴, Boris Straumal ^{2,5,6,*}, Gennady Salishchev ⁷ , Almagul Mansharipova ⁸, Aigul Kabiyeva ⁹, Maratbek Gabdullin ¹⁰, Sergey Dobatkin ^{2,3} and Yuri Estrin ^{11,12} 

- ¹ N.N. Blokhin National Medical Research Center of Oncology of the Ministry of Health of the Russian Federation (N.N. Blokhin NMRCO), 115478 Moscow, Russia; n_anisimova@list.ru (N.A.); nkeryam@gmail.com (K.N.); kisele@inbox.ru (M.K.)
- ² Laboratory of Functional Polymeric Materials, Department of Physical Metallurgy and the Physics of Strength, National University of Science and Technology "MISIS", 119991 Moscow, Russia; dobatkin.sergey@gmail.com
- ³ A.A. Baikov Institute of Metallurgy and Materials Science of the RAS, 119334 Moscow, Russia; nataliasmartynenko@gmail.com (N.M.); rybalch@mail.ru (O.R.)
- ⁴ P.N. Lebedev Physical Institute of the RAS, 142432 Moscow, Russia; rybalchenkov@lebedev.ru
- ⁵ Institute of Nanotechnology, Karlsruhe Institute of Technology, 76344 Eggenstein-Leopoldshafen, Germany
- ⁶ Institute of Solid State Physics and Chernogolovka Scientific Center of the Russian Academy of Sciences, 142432 Chernogolovka, Russia
- ⁷ Laboratory of Bulk Nanostructured Materials, Belgorod National Research University, 308015 Belgorod, Russia; Salishchev_G@bsu.edu.ru
- ⁸ Department of Scientific and Clinical Work, Kazakh-Russian Medical University, Almaty 050000, Kazakhstan; dralma@mail.ru
- ⁹ Association of Early Career Doctors of Almaty, Almaty 050000, Kazakhstan; kabiyeva.20011@yandex.ru
- ¹⁰ Kazakh British Technical University, Almaty 050000, Kazakhstan; m.gabdullin@kbtu.kz
- ¹¹ Department of Materials Science and Engineering, Monash University, Clayton, VIC 3800, Australia; yuri.estrin@monash.edu
- ¹² Department of Mechanical Engineering, The University of Western Australia, Perth, WA 6009, Australia
- * Correspondence: straumal@issp.ac.ru



Citation: Anisimova, N.; Martynenko, N.; Novruzov, K.; Rybalchenko, O.; Kiselevskiy, M.; Rybalchenko, G.; Straumal, B.; Salishchev, G.; Mansharipova, A.; Kabiyeva, A.; et al. Modification of Biocorrosion and Cellular Response of Magnesium Alloy WE43 by Multiaxial Deformation. *Metals* **2022**, *12*, 105. <https://doi.org/10.3390/met12010105>

Academic Editor: Guy Ben-Hamu

Received: 23 November 2021

Accepted: 28 December 2021

Published: 5 January 2022

Publisher's Note: MDPI stays neutral with regard to jurisdictional claims in published maps and institutional affiliations.

Abstract: The study shows that multiaxial deformation (MAD) treatment leads to grain refinement in magnesium alloy WE43. Compared to the initial state, the MAD-processed alloy exhibited smoother biocorrosion dynamics in a fetal bovine serum and in a complete cell growth medium. Examination by microCT demonstrated retardation of the decline in the alloy volume and the Hounsfield unit values. An attendant reduction in the rate of accumulation of the biodegradation products in the immersion medium, a less pronounced alkalization, and inhibited sedimentation of biodegradation products on the surface of the alloy were observed after MAD. These effects were accompanied with an increase in the osteogenic mesenchymal stromal cell viability on the alloy surface and in a medium containing their extracts. It is expected that the more orderly dynamics of biodegradation of the WE43 alloy after MAD and the stimulation of cell colonization will effectively promote stable osteosynthesis, making repeat implant extraction surgeries unnecessary.

Keywords: magnesium alloy; multiaxial deformation; biodegradation; cell viability; cell colonization



Copyright: © 2022 by the authors. Licensee MDPI, Basel, Switzerland. This article is an open access article distributed under the terms and conditions of the Creative Commons Attribution (CC BY) license (<https://creativecommons.org/licenses/by/4.0/>).

1. Introduction

The development of biodegradable implants for clinical practice is a pressing task of modern medicine. Specifically, the development of medical devices of this type is relevant for osteosynthesis in orthopedics, as well as in oral and cranio-maxillofacial surgery to eliminate the consequences of injuries, tumor formation and hypoplasia both in adult patients and in children [1–3]. The choice between the use of biodegradable and non-biodegradable implants must be carefully considered. Traditional biodegradable submersible medical devices for osteosynthesis have been successfully used in bone reconstruction with low or

moderate stress. The advantage of biodegradable bone implants is that their dissolution eliminates the need for repeat surgeries to remove the implant after bone healing is completed. One should also not overlook further benefits of the use of bioresorbable implants over traditional devices based on titanium alloys, such as a higher radio transparency and a lower mechanical load during their service life. Indeed, the implants based on biodegradable materials gradually transfer the load onto the remodeled bone as they degrade [4]. For use in biodegradable medical devices, polymers, ceramics, or biodegradable alloys are considered. Several complications inhibit their implementation in biomedical products, however. These include their usually low mechanical strength and instability, tardy or excessively rapid biodegradation, and insufficient biocompatibility. The difficulties are compounded by the limited availability of bioresorbable materials approved for clinical use [5,6].

It is known that the use of polymer-based implants in clinical practice, in contradistinction to metal implants, is limited due to the potential rapid loss of the initial strength, resulting in a high risk of recurrent fractures. In this case, an inappropriate selection of the material for the biodegradable implant may lead to a deterioration of its performance and severe complications such as sterile abscess and osteolysis. This would call for additional surgery to remove or replace the implant, thus negating the prime advantage of using biodegradable alloys for osteosynthesis [5–7]. Clinical trials of polymer-based bioresorbable fixation screws in maxillofacial surgery [7,8] showed that their perioperative failure occurred much more often than that of titanium-based screws. Due to these issues with bioresorbable polymeric osteosynthetic materials, there is a demand for materials with higher strength that offer advantages over a combination of mechanical properties, and magnesium alloys are in the spotlight as materials that can meet this demand [4]. However, the rapid corrosion of magnesium alloys, coupled with the accumulation of gaseous hydrogen and a sharp rise of local pH, hinders the application of magnesium-based implants into clinical practice. One of the magnesium alloys most widely used for medical applications, mainly for coronary stents [9,10], is the WE43 alloy. To enable the use of WE43 for orthopedic purposes, several ways to improve its properties were proposed. Oshibe et al. [11] showed that anodization slowed the corrosion of WE43 implants and the hydrogen gas evolution after intraosseous implantation. In an earlier study [12], we showed that the mechanical treatment of homogenized WE43 by equal channel angular pressing (ECAP), rotary swaging (RS), and multiaxial deformation (MAD) significantly improved the mechanical properties of the initial alloy, enhanced its biocompatibility, and also reduced the rate of biodegradation both *in vitro* and *in vivo*. The results obtained highlight the greatest promise of the mechanical treatment of the WE43 alloy by MAD for its successful use in fasteners, screws, and intraosseous implants for osteosynthesis. For such applications, it is often necessary to reduce the rate of biodegradation of the material, especially in the early stages of the process, in order to allow for sufficient time for the completion of osteosynthesis in the bone reconstruction area. MAD was shown to increase the strength and corrosion resistance of the WE43 alloy, while also enhancing its ductility, which is no less important for the manufacture of orthopedic devices [13].

Building on the success of the foregoing study, the aim of the present work is to provide an in-depth assessment of the effect of the mechanical treatment of the WE43 alloy by MAD in an attempt to improve the spectrum of its properties. The ultimate goal of this research is to develop a knowledge base for its use in implantable devices for orthopedics. Specifically, the focus is on the variation in the microstructure and corrosion properties of the alloy, as well as on detailed analysis of the dynamics of its biocorrosion and bioactivity in various simulated body fluids *in vitro*.

2. Materials and Methods

2.1. Material Investigated

The investigation was carried out on magnesium alloy WE43 (Mg–3.56%Y–2.20%Nd–0.47%Zr). The alloy was obtained by melting in an induction furnace using high-purity

magnesium and industrial alloys of rare-earth metals and zirconium under a protective gas mixture at a temperature of 750 °C. An alloy ingot with a diameter of 64 mm was cooled in air and then homogenized at a temperature of 525 °C for 8 h—a thermal treatment that brings the structure into thermodynamic equilibrium. To obtain the initial rods of the required diameters for subsequent deformation, the ingot was extruded at a temperature of 430 °C to a final diameter of 25 mm. The rods thus obtained were annealed again at a temperature of 525 °C for 8 h. They were then cooled in air to create a supersaturated solid solution of rare earth metals in magnesium. Henceforth, this alloy state will be considered as a reference state, denoted as WE43 Hom. Starting from this initial state, MAD of cylindrical samples with a diameter of 25 mm and a height of 40 mm was carried out with a stepwise decrease in the processing temperature from 450 °C to 300 °C (in 25 °C steps and four passes at each temperature point). The total of 28 MAD cycles corresponded to a total strain of 17.5. In what follows, this alloy state will be denoted as WE43 MAD. The study of the microstructure of the alloy in the initial state, as well as changes in the surface morphology of the samples after corrosion tests, was carried out using a scanning electron microscope (SEM) JSM-7001F (JEOL, Tokyo, Japan) equipped with an EDS attachment. The microstructure of the alloy after MAD was investigated using transmission electron microscopy on a JEM-1400 electron microscope (JEOL, Tokyo, Japan) operating at a voltage of 120 kV. The size of the microstructural entities was measured by the random secant method using the Image Expert Professional 3 software. The mechanical properties of the alloy were investigated on an Instron 3382 testing machine using cylindrical specimens with a diameter of 3 mm, a total length of 33 mm and a working length of 15 mm.

Before beginning the study of the biodegradation and incubation with cells, the alloy samples were immersed for 3 h in 70% ethanol for sterilization and then dried in a sterile atmosphere.

2.2. Accumulation of Biodegradation Products in a Bioactive Medium

To study the kinetics of degradation, an xCELLigence RTCA Systems analyzer (ACEA Biosciences Inc., Santa Clara, CA, USA) and special 16-well plates (E-plate 16, ACEA Biosciences Inc.) were used. By this method, changes in the electrical impedance (ΔI) due to the accumulation of degradation products of the sample are measured against the baseline of the impedance of the culture medium (Figure 1). This is performed in real time using a biosensor located at the bottom of each well. In the wells of the plate, 50 μ L of the immersion medium was added and a common baseline of the signal was defined. After adding 150 μ L of an additional portion of the immersion medium, the test alloy samples ($n = 4$) were placed in the wells vertically so that they, whilst being immersed in the corrosion medium, did not touch the bottom (Figure 1). As the immersion medium, fetal bovine serum (FBS) (HyClone, Thermo Fisher, Horsham RH12 4QD, UK) or the complete growth medium based on Dulbecco's Modified Eagle's Medium (DMEM) (Sigma-Aldrich, St. Louis, MO, USA) supplemented with 10% FBS, 4 mM L-glutamine (PanEco, Moscow, Russia) and 1% penicillin/streptomycin (PanEco, Moscow, Russia) were used. The magnitude of ΔI was measured in duplicate every 15 min during 288 h of incubation of the samples in an immersion medium at 37 °C in an atmosphere of 5% carbon dioxide. Every two days, a 50 μ L portion of fresh complete corrosion medium was added to each well.

2.3. pH Variation in the Immersion Medium

Alloy samples ($n = 3$) were incubated in 2 mL FBS or the complete growth medium for 1 day at 37 °C in an atmosphere of 5% carbon dioxide. Then, the immersion medium was taken for pH analysis, and the same quantity of a fresh immersion medium was added to the tube. The total duration of incubation of alloy samples in the immersion medium was 12 days. The pH was measured in triplicate using a pH 211 Microprocessor Meter (Hanna Instruments, Vöhringen, Germany).

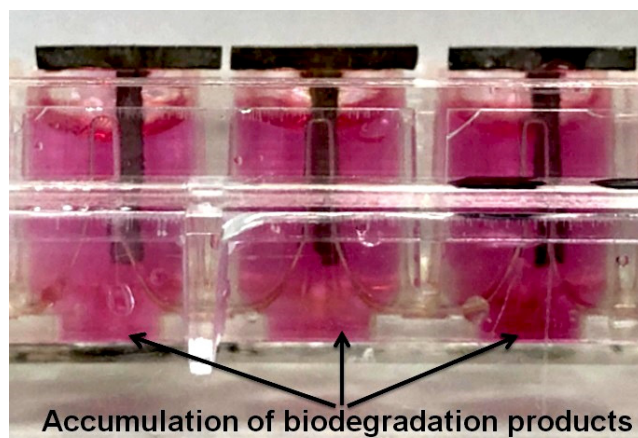


Figure 1. Accumulation of biodegradation products of samples of alloy WE43 in initial state and after MAD in the immersion medium. The samples were placed in the wells of the special 16-well plates vertically so as to be partially immersed in the fetal bovine serum or the complete growth medium, and did not touch the bottom. The plate with alloy samples was incubated in the xCELLigence RTCA Systems analyzer at 37 °C in an atmosphere of 5% carbon dioxide. The device measured an electrical impedance (ΔI) due to the accumulation of alloy degradation products at well bottom every 15 min for 288 h.

2.4. Volume CT Scan and Magnitude of Hounsfield Units

Alloy samples ($n = 3$) were incubated in 2 mL FBS for 13 days at 37 °C in an atmosphere of 5% carbon dioxide. The immersion medium was replaced daily. Alloy samples were analyzed daily using a Quantum GX2 microcomputer tomograph (Ridaku Vicro CT Technology, Perkin Elmer, Yokohama, Japan) at 90 kV, 88 μ A, FOV 36 mm, slice thickness 36 μ m. The data were analyzed using Analyze 14.0 software (AnalyzeDirect Inc., Stilwell, KS, USA). The results of alloy volume CT scan measurement after incubation in the FBS were presented as a percentage of the initial value. Hounsfield unit (HU) values of the alloys were also measured. As it is known, the Hounsfield scale is a quantitative scale for describing radiodensity.

2.5. Mass Loss after Incubation in FBS and in the Complete Growth Medium

Alloy samples were incubated in 2 mL complete growth medium for 6 days or in FBS for 12 days at 37 °C in an atmosphere with 5% carbon dioxide. The immersion medium was changed daily. The weight of alloy samples ($n = 3$) was measured before the start of the experiment and after the end of the incubation period using an OHAUS PR223/E analytical balance (OHAUS Corp., Parsippany, NJ, USA). The results are presented as a percentage of sample weight loss relative to the initial value.

2.6. Cytotoxicity, Cell Viability and Proliferation

The studies were carried out using mouse bone marrow mesenchymal multipotent stromal cells (MMSCs) (cell cultures collection of N.N. Blokhin NMRCO). Cells in the logarithmic growth phase were treated with trypsin, washed with DMEM, and resuspended in complete growth medium at a concentration of 600,000 cells/mL.

To assess the effect of the alloy on cell viability and proliferation, MMSCs were incubated on the surface of the alloy samples. For this purpose, 20 μ L of the cell suspension was seeded on the surface of alloy samples and incubated at 37 °C in an atmosphere with 5% carbon dioxide. Thirty minutes later, 2 mL of complete growth medium was carefully added to the wells containing alloys with cells and further incubated for 7 days under the same conditions. Every day, the old cell medium was removed and replaced with a portion of fresh complete growth medium. Before collecting the incubation medium, the plates were gently shaken. The collected incubation medium was centrifuged at 300 \times g for 5 min. The cytotoxicity of the alloys was assessed by measuring the extracellular activity of lactate

dehydrogenase (LDH release) in the incubation medium supernatants. The cell viability was calculated as the LDH activity of MMSC after their incubation with the alloys for 7 days. The analysis was conducted using the Lactate Dehydrogenase Activity Assay Kit (Merck, Sigma-Aldrich, St. Louis, MO, USA) according to the manufacturer's guidelines. The optical density (OD) was measured at a wavelength of 492 nm with a reference at 620 nm (OD492-OD620) using the Spark[®] Multimode Microplate Reader (Tecan, Baldwin Park, CA, USA).

To assess cell colonization, MMSCs were incubated in the wells of a 24-well plate (Nunc-Nuclon, Waltham, MA, USA) for 7 days in a complete growth medium containing 10% extracts of the studied alloys, and on the surface of alloy samples as described above. To obtain extracts, the alloy samples were incubated one by one in 2 mL of complete growth medium for 5 days at 37 °C in an atmosphere with 5% carbon dioxide. Then, the seeded cells were washed from the old growth medium, stained with Live/Dead Cell Double Staining Kit (R & D, Sigma-Aldrich, Burlington, MA, USA) and Hoechst (Invitrogen, Waltham, MA, USA), and analyzed using a Lionheart FX automated microscope (BioTek, Santa Clara, CA, USA).

2.7. Statistical Analysis

All statistical analyses were carried out using Statistica 6.0 (StatSoft, Tulsa, OK, USA). Differences among the groups of samples were analyzed by using one-way ANOVA. The data are presented as mean \pm standard deviation (SD). Results are considered statistically significant for $p < 0.05$.

3. Results

3.1. Study of the Microstructure

Figure 2 illustrates the SEM microstructure of the WE43 Hom. alloy. It is seen that in the homogenized state, the alloy consists of equiaxed grains of solid solution with an average size of $55.05 \pm 1.73 \mu\text{m}$. In addition, the structure is dotted with precipitated phase particles aligned line-wise along the direction of the last extrusion step (Figure 2b). Elemental scanning showed that some of these precipitates are rich in yttrium (rectangular precipitates), while others are rich in neodymium (rounded precipitates). Both types of precipitates contain oxygen and practically do not contain magnesium (Figure 2b,c). These precipitates are probably oxides of yttrium (Y_2O_3) and neodymium (Nd_2O_3). In addition, segregations of Zr arranged line-wise are observed. No presence of Mg compounds with rare earth metals was detected.

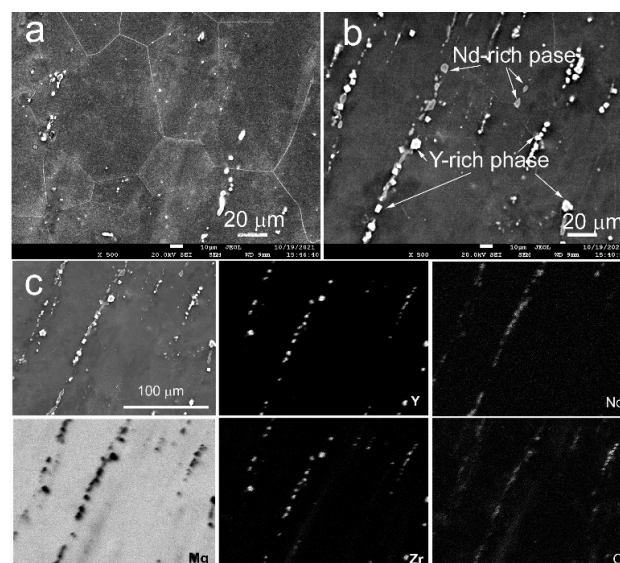


Figure 2. SEM structure of the alloy WE43 in the initial state (a,b) and elemental mapping (c).

MAD is seen to have resulted in a significant microstructure refinement. As a result of deformation, the average grain size dropped to $0.93 \pm 0.29 \mu\text{m}$ (Figure 3a). At the same time, predominantly point reflections on the rings of the electron diffraction pattern indicate the formation of a coarse grain structure with high-angle boundaries (Figure 3b). No line-wise arranged precipitates were recorded in this case. It could be surmised that heating involved in the processing and severe deformation the material underwent led to the dissolution of precipitates present in the microstructure of the initial WE43 Hom. alloy. However, in the microstructure of the WE43 MAD alloy, the precipitation of rounded $\text{Mg}_{41}\text{Nd}_5$ particles with an average size of $0.34 \pm 0.21 \mu\text{m}$ was observed. The loss of these particles is due to a combination of pre-heating for processing and the deformation process itself (Figure 3c,d).

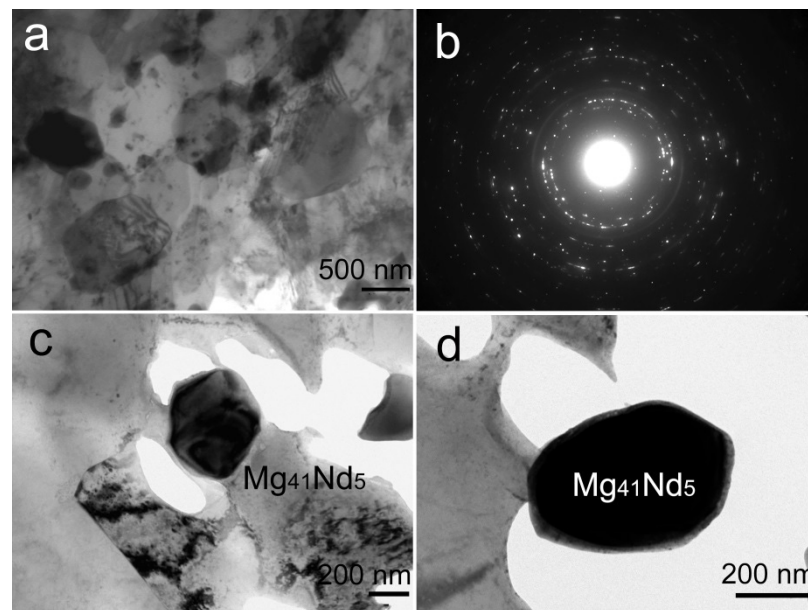


Figure 3. The structure of the WE43 alloy after MAD (a), as well as the diffraction pattern from the image obtained (b); particles of the $\text{Mg}_{41}\text{Nd}_5$ phase (c,d).

As mentioned earlier in [13], the formation of an ultrafine-grained (UFG) structure caused by MAD led to an increase in the yield stress (YS) of the alloy from 161 MPa in the initial state to 210 MPa after MAD. The ultimate tensile strength (UTS) in this case increased from 234 MPa to 300 MPa. The tensile elongation (EI) of the WE43 MAD alloy increased from 9.0% in the initial state to 17.2%.

3.2. Accumulation of Biodegradation Products in a Bioactive Medium

The data obtained demonstrate a different profile of the dynamics of the accumulation of biodegradation products of the alloy samples in a corrosion medium represented by FBS and a complete growth medium based on DMEM containing only 10% FBS. In the first case, an accelerated increase in the intensity of this process was observed already on the second day of incubation, after which a progressive slowdown in the dynamics of ΔI was observed. The maximum level was reached on the 5th–6th day, after which no significant change in the recorded data was observed. The biocorrosion process in the growth medium proceeded in a completely different way. Signs of the uniform accumulation of degradation products of the WE43 Hom. alloy were observed at the bottom of the wells during the entire observation period, up to their stabilization after 9–10 days (Figure 4a,b). A periodic short-term increase in the ΔI values, noticeable in both serrated graphs, is associated with the recurrent addition of fresh portions of the corrosive medium to the wells during incubation.

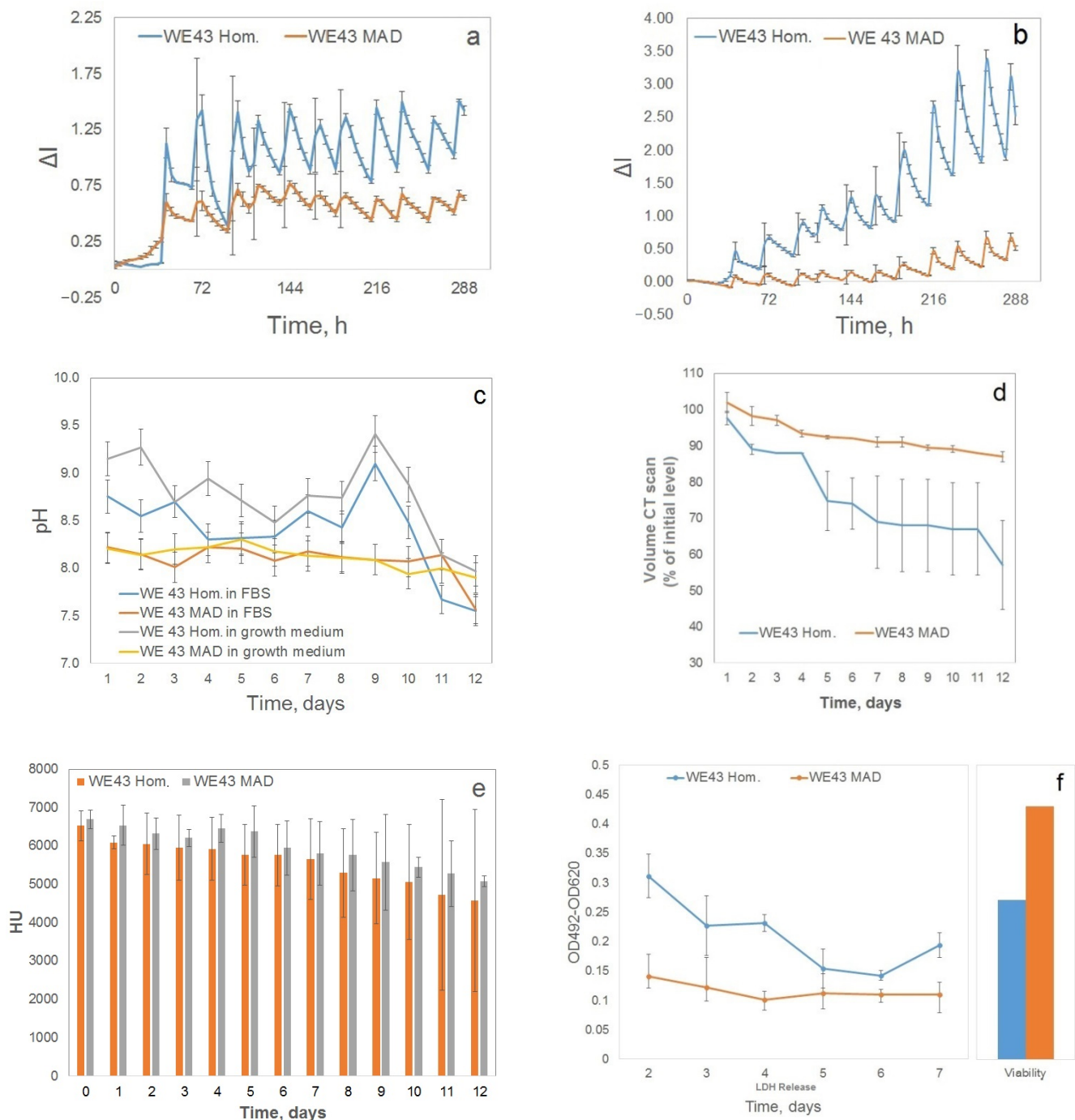


Figure 4. Dynamic of the accumulation of biodegradation products for WE43 Hom. and WE43 MAD in fetal bovine serum (a) and in complete growth cell culture medium (b). The dynamic of the pH value of the corrosion environment for alloys WE43 Hom. and WE43 MAD in FBS and in complete growth medium (c). Variation in the volume CT scan during incubation in FBS (d). The dynamic of Housefield unit values of the samples during the incubation of alloy samples in FBS (e). Dynamic of the cytotoxicity of WE43 alloy samples in initial state and after MAD according to the results of the LDH release, and the cell viability after 7 days of incubation of MMSCs seeded on alloys according to the LDH activity data (f). Data are presented as a mean \pm SD.

A different picture of biodegradation was observed for the MAD-processed alloy. The accumulation of its biodegradation products at the bottom of the wells was much slower. A significant increase in ΔI was detected only after 6 days from the start of the

experiment. Thus, the treatment of the WE43 alloy by MAD led to a delay in the onset of the formation of biodegradation products, a smoother course of the biocorrosion process, and its overall deceleration.

3.3. Variation in pH of Incubation Medium

For this study, the samples were incubated in equal volumes of a model bioactive corrosive medium (FBS or the complete growth medium). After 1 day of incubation, the medium was completely removed, and its pH was measured; the same volume of fresh FBS or complete growth medium based on DMEM was added to alloys to continue the corrosion process (Figure 4c).

It is noteworthy that pH fluctuations in FBS due to the biodegradation of alloys were significantly weaker in comparison with DMEM. This can be associated with a higher concentration of proteins with a large buffer capacity due to amphotericity in the case of FBS. The homogenized alloy alkalized the corrosive medium much more strongly than the MAD-processed one. Furthermore, already after one day from the start of WE43 Hom. incubation, the pH of the complete growth medium rose to 9.5, which indicates a rapid onset of the biodegradation process. In the FBS, this parameter value for the same time was lower (pH = 8.5). During further incubation of WE43 Hom. in both corrosion media, their pH changed abruptly, reaching peak values on the 8th–9th day of observation (Figure 5). Subsequently, the intensity of the effect of this alloy on the pH medium dropped off significantly. The alkalization of the corrosion medium was less pronounced under the influence of the MAD-modified alloy. The dynamics of this indicator in both media did not differ too much (Figure 4c). In general, a steady increase in the pH value of medium was observed over most of the observation period. This indicates a continual biodegradation process after MAD mediating the uniform release of hydrogen anions from the alloy during corrosion. The observed deceleration of this process with the incubation time promoted a tendency of the pH to be maintained at a neutral level. This stabilization occurred after about 11 days of incubation in FBS, to be compared with the complete growth medium where it took about 8 days.

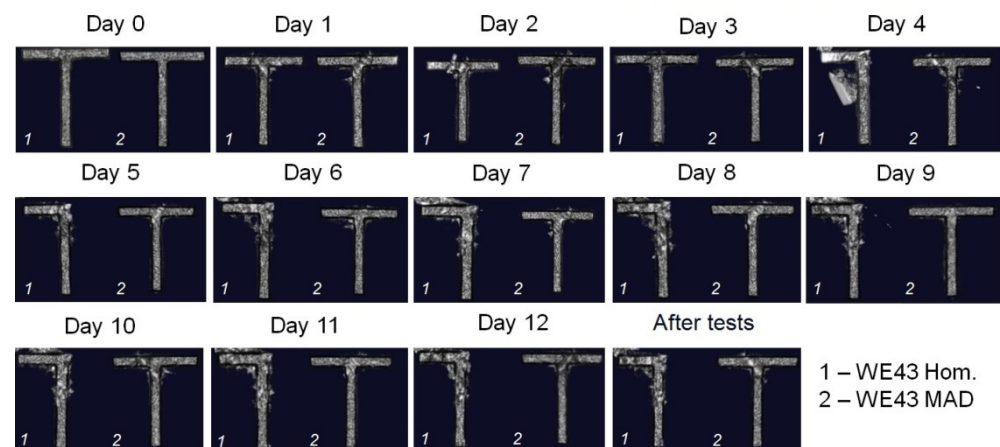


Figure 5. Degradation of WE43 alloy samples in the initial and MAD-modified states during incubation in FBS (the immersion medium was changed daily).

3.4. Volume CT Scan and Magnitude of Hounsfield Units in FBS In Vitro

The study of the change in the volume CT scan of the alloy samples immersed in FBS in vitro is presented in Figures 4d and 5.

Volume CT scan measurements showed that a decrease in the parameter value of the samples based on the alloy in initial state occurred much faster than that of the samples treated by MAD. As shown in Figure 5, already on day 4, the disintegration of some of the samples of the homogenized material was observed. On the 5th day of incubation, all homogenized alloy samples had signs of deterioration localized in different areas. The

frontal section obtained by the method of computer tomography indicates a significant inhomogeneity of the X-ray density (radiodensity) of the homogenized alloy. These data show that biocorrosion led to the rapid destruction of the sample in areas with the lowest radiodensity (Figure 4e).

These results are supported by the data of the HU measurements, which show that after MAD, the alloy had a higher radiodensity than the homogenized one, which, obviously, is a consequence of a change in its microstructure. During the biocorrosion experiments, the overall HU values of the samples decreased, which was probably caused by the oxidation of the alloy and the accumulation of degradation products on their surface. It is worth noting that the radiodensity of the homogenized samples showed a tendency to continually decrease after the second day of incubation, while the MAD-processed samples maintained the stability of radiodensity over 5 days, after which time a gradual decrease in HU values set in.

3.5. Study of Alloy Degradation Products

Figures 6 and 7 illustrate the results of studying the alloy surface in initial and MAD-modified states after 12 days of incubation in FBS. After this exposure to a corrosive medium, the surface of alloy samples in both states was covered with a thick layer of needle-shaped crystals. Elemental scanning of these crystals showed that they mainly consisted of Mg and O. This suggests a conclusion that they were mostly magnesium oxide (MgO) crystals.

The presence of Nd and Y in the composition of the degradation products, probably stemming from the matrix, was also detected. In addition, such elements as Na, Cl, Ca, and K were also found in the film (Figures 6c and 7c). Their provenance may be associated with the protein-rich medium (FBS) [14].

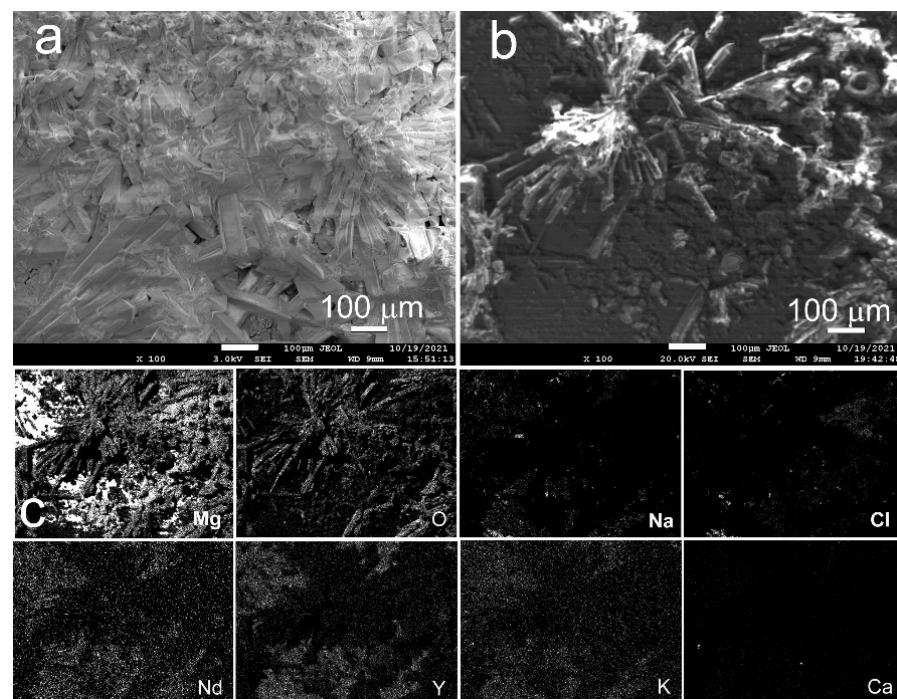


Figure 6. Appearance of degradation products of WE43 Hom. (a,b) and elemental mapping (c) after 12 days of incubation in FBS.

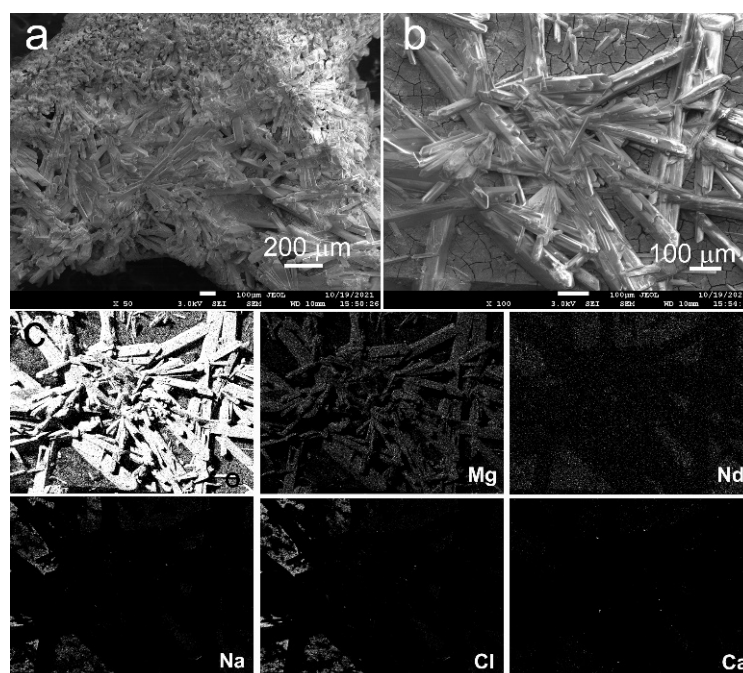


Figure 7. Appearance of WE43 MAD degradation products (a,b) and elemental mapping (c) after 13 days of incubation in FBS.

3.6. Mass Loss after Incubation in FBS and DMEM

The mass loss measurements described in Section 2.5 returned data that can be summarized as follows. The mass loss of the homogenized samples was greater than that of the samples of the MAD-modified alloy. The duration of incubation in the growth medium based on DMEM was 6 days, and the difference in weight loss between the samples was insignificant ($p > 0.05$). However, after incubation of the samples in FBS for 12 days, the difference in the mass loss of the samples was substantial: the mass of the samples relative to the initial value was $72 \pm 2\%$ before and $97 \pm 2\%$ after MAD treatment.

3.7. Cytotoxicity

To evaluate the cytotoxicity of the alloy in both microstructural states, LDH release was assessed. It is known that LDH is an intracellular enzyme and its appearance in the extracellular environment means damage to the cell membrane, which serves as a marker of cytotoxicity of the influencing factor. In this study, MMSCs with osteogenic potential were incubated on the surface of alloy samples. The growth medium was changed daily and the LDH release was assessed. To evaluate the viability of the MMSC on the alloy sample surface, the cell LDH activity was assessed after 7 days of cultivation (Figure 4f). The presented graphs demonstrate that the highest cytotoxic effect occurred at the beginning of co-incubation, and then the level of the LDH release decreased, thus reflecting a tendency for the cytotoxicity of the alloy to diminish. Comparative analysis showed that the cytotoxicity of the alloy after MAD was significantly less expressed than that of the homogenized alloy. These results are consistent with the data showing a decrease in the cytotoxicity of the WE43 alloy after treatment with MAD to white blood cells obtained earlier [13].

In cell colonization assays, MMSCs were incubated not only on the surface of alloy samples, but also in a medium containing their extracts (Figure 8). The data obtained demonstrate that cell survival in the medium with a MAD-modified alloy extract was significantly higher than in that with a homogenized alloy extract. The presence of a larger number of active cells on the MAD-modified alloy surface signifies a stimulating effect of the alloy on cell adhesion and colonization.

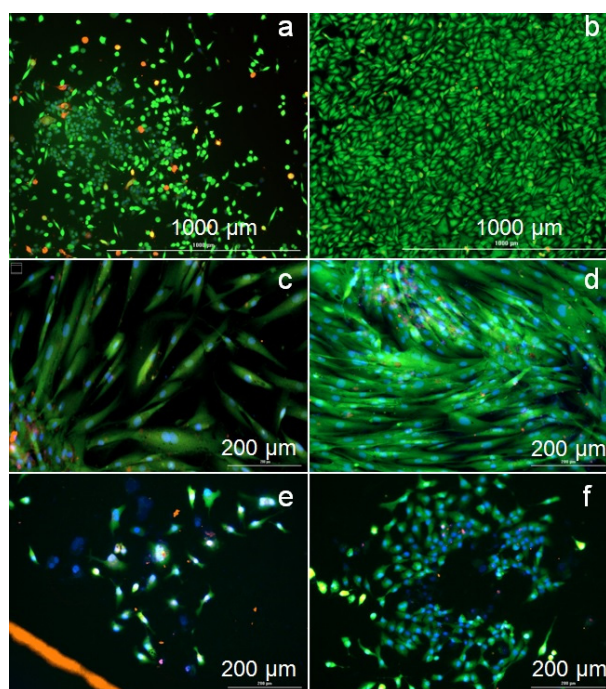


Figure 8. MMSCs cultivated in a medium containing the extracts of WE43 Hom. (a,c) and WE43 MAD (b,d) at different magnifications: $\times 100$ (a,b) and $\times 200$ (c,d), and on the surface of alloy samples based on WE43 Hom. (e) and WE43 MAD (f). Cell staining with the Live/Dead Double Staining reagent kit (Sigma, Ronkonkoma, NY, USA): live cells—green color, dead cells—red color. Cell nuclei were stained with Hoechst—blue color.

4. Discussion

The study of the intensity of the biodegradation of WE43 alloys before and after treatment with MAD, in media with different protein concentrations (FBS and the complete growth medium containing only 10% FBS), showed that this process was more pronounced in FBS, which was similar in biochemical, physiological, and physical characteristics to human blood serum. The data obtained indicate unambiguously that the corrosion of MAD-modified WE43 alloy in a bioactive medium with a high protein content was inhibited compared with that of the alloy. Jonson et al. [15] also reported that proteins can enhance or inhibit the decomposition of Mg alloys depending on various factors. They noted that there is no consensus in the literature on the origin of their modifying action. In particular, the authors suggested that proteins may be the main factor governing the biodegradation of Mg alloys, but the details of this effect have yet to be investigated. The article [15] reported the effect of FBS on the decomposition of magnesium and magnesium-based alloys. It was found that FBS had little effect on the mass loss of pure magnesium samples during immersion, regardless of whether a natural oxide layer was present on the sample surface or not. FBS reduced the mass loss of the magnesium–yttrium (MgY) alloy with an oxidized surface during immersion degradation but increased the mass loss of the same alloy with a bare metal surface. FBS also influenced the character of degradation by limiting the depth of pitting corrosion during the fracture of commercially pure Mg with bare or oxidized surfaces and on MgY alloy with oxidized surfaces. The authors demonstrated that blood serum proteins interact intensively with biodegradable magnesium-based alloys, and the result of this interaction can be tuned by changing the alloy composition and details of processing. It was assumed that the adsorption of proteins on the surface of alloys through electrostatic or hydrophobic interactions depends on the roughness of the alloy surface, its physical properties, and chemical composition. In another, earlier work by the same authors, data were presented showing that the corrosion rate of magnesium alloys can also be significantly influenced by functionally active ions (physiological salt ions), which

are present in FBS, but absent in distilled water [16]. The effect was associated with the influence of these ions on the conformational structure of the proteins in the environment, thereby changing its biological activity.

It is known that due to amphotericity (the presence in the molecule of both acidic and basic R groups of dicarboxylic and diamine amino acid residues), proteins are usually concentrated at the interfaces, which can cause the formation of a concentrated protein layer on the surface of the alloy sample. This process can be intensified due to the interaction of the protein with the surface oxide layer or its sedimentation on the implanted device surface [17,18]. A layer of protein adsorbed on the alloy can act as a physical barrier that protects the surface from contact with electrolytes and aggressive ions, and can inhibit cathodic half-reactions by blocking cathode sites [19,20]. Negatively charged proteins are more strongly attracted to the cathodic sites of the corroding alloy and can inhibit its degradation, competing with chlorine ions for adsorption on the alloy surface [21]. At the same time, the presence of a layer of protein adsorbed on the surface of the magnesium alloy cannot completely suppress its biodegradation, since the interposition of protein chains forms pores that provide access for electrolytes and aggressive ions to the surface of the alloy. Hence, it can be concluded that an increase in the concentration of protein in the immersion medium can facilitate the formation of a more effective barrier that protects the alloy from intensive corrosion. However, an opposite effect is also possible. Some proteins, when adsorbed on the surface of the alloy, rearrange themselves, contacting the surface of the sample with the hydrophobic part of the molecule [22] and catalyzing the oxidation of metals by contact with the internal disulfide bridges of molecules of globular proteins (for example, albumin) [23]. Moreover, the effect exerted on the degradation rate depends both on the nature of the metal surface and on the considered protein [24].

Thus, the presence of proteins or physiological salt ions, as well as their concentration in the medium in contact with the implant, should be considered when predicting the rate of degradation of a magnesium-based medical device in model body fluids *in vitro* or in a patient's body. The different intensity of biocorrosion in a protein medium of alloys before and after severe mechanical treatment may be associated with the difference in the incidence of active groups on the surface of the alloy. Specifically, grain refinement by MAD and variation in the occurrence of the constituent elements on the surface of the alloy may be responsible for differences in the response of WE43 to a protein medium. Our microstructure investigations showed that the grain size of alloy WE43 was reduced by MAD by a factor of 50, down to a UFG state. In addition, the precipitates of Y and Nd oxides arranged line-wise in the homogenized alloy were eliminated by MAD (probably due to additional heating and a severe deformation of the material). The presence of such precipitates in magnesium alloys is undesirable, as they tend to provoke the nonuniformity of the corrosion process, which we observed in the case of WE43 Hom. The microstructure produced by MAD processing is more favorable: it is fine grained (~1 μm) and contains more corrosion-resistant particles of the $\text{Mg}_{41}\text{Nd}_5$ phase, evenly distributed in the matrix. As reported in the literature, the formation of a uniform UFG structure can improve the corrosion resistance of magnesium alloys [25–28]. In our case, the uniformity of the distribution of the $\text{Mg}_{41}\text{Nd}_5$ particles did not cause the occurrence of inhomogeneity of corrosion, suggesting that the formation of cathode–anode pairs with the metal matrix was not an issue here [29,30].

According to the results of microCT, the WE43 alloy in its initial state had a lower radiodensity than WE43 alloy after MAD. Furthermore, as the incubation period increased, we observed that the X-ray density of homogenized alloy dropped off faster compared with that of the MAD-processed alloy. In addition, the degradation of the MAD-modified alloy samples in an initial incubation period was slower. The analysis of the sections obtained using microCT showed that the sites of destruction, which led to the formation of sample fragments, appeared in the regions of the WE43 Hom. alloy with reduced X-ray density. This is believed to have caused the multifocal nature of the destruction of this alloy with the initial formation of local corrosion pits, gradually penetrating the bulk of

the sample and finally leading to the failure of the device. After the treatment by MAD, the size of the low-radiodensity zones diminished significantly, which can be associated with the microstructural changes described above. One of the important outcomes of the present investigation is the recognition that the character of corrosion of the WE43 alloy changed after treatment by MAD. Prior to treatment, the corrosion process developed locally, forming pits on the surface of the material [31]. By contrast, after the MAD treatment, a more uniform corrosion due to a much finer distribution of grain boundaries facing the alloy surface was observed. Interestingly, as mentioned above, the occurrence of potential galvanic corrosion due to the presence of precipitated second-phase particles did not seem to be an issue disrupting the homogeneous character of corrosion. As a result, the decrease in the volume of alloy samples with MAD processing was slow and smooth, unlike the rapid, abrupt biodegradation of a homogenized sample. Similarly, it is the difference in the character of biodegradation, which caused a much more pronounced alkalization of the immersion medium by the alloy in a homogenized state. This accounts for its greater cytotoxicity, which led to a decrease in the cell viability, as well as the adhesion and proliferation of MMSCs with osteogenic potential on its surface. In addition, the increase in the bioactivity of the alloy after MAD may be associated with the uniform sedimentation of the protein from the growth medium. This adsorbed protein, forming a more or less uniform substrate on a large surface of a MAD-modified alloy sample, may indirectly stimulate cell adhesion and proliferation, as well as prevent the shedding of MMSCs from the surface and hinder hydrogen evolution. This is an obvious improvement over the situation in the homogenized condition, where the formation of a more contiguous protective protein film is precluded by the local character of the corrosion sites. In earlier work, we already showed that mechanical treatment of the WE43 alloy by another technique of severe plastic deformation, referred to as rotary swaging, gave rise to a modification of its bioactive properties, inhibiting the surface adhesion of yeast cells [32]. The more intense proliferation of MMSC incubated in the medium with alloy extracts, in comparison with the activity of cells seeded directly on the samples, can be explained by the formation of needle-like crystals on their surface, which are biodegradation products of the WE43 alloy. Due to their shape, these crystals can mechanically damage cells and prevent their adhesion. The high degree of cell viability and colonization in the presence of an extract of the WE43 MAD alloy indicates the low level of toxic agents released in the growth medium from this alloy during its degradation. At the same time, a decrease in cell viability under the influence of an extract of the homogenized WE43 alloy, despite its similar chemical composition, may be due to a higher degree of alkalization of the cell growth medium. Thus, there are sufficient grounds to assume that the decrease in the MMSCs viability and the intensity of their colonization of the homogenized alloy surface is largely due to two major factors: (i) the deterioration of the properties of the growth medium, notably due to an increase in pH, and (ii) mechanical damage to cells by crystals of the products of the biodegradation of alloys.

The observed change in the speed of the variation in the volume CT scan and mass loss of the alloy samples during biocorrosion in FBS effected by MAD was remarkable. The gradual slow decrease in the MAD-modified sample volume CT scan contrasted with the precipitous biodegradation of the homogenized samples. This provides an explanation for the previously discovered effect of the inhibition of biodegradation *in vivo* of the WE43 alloy by MAD processing [12]. It should be noted that failure of the homogenized WE43 alloy samples occurred in the bulkhead regions, that is, locations more susceptible to corrosive effects. This allows one to predict the potential failure sites within a future finished product made from alloy in the initial state. Such information is indispensable for implant design and the prediction of their reliability. For example, the probability of breakage of the threaded part of a screw made from WE43 alloy after MAD will be substantially lower than for a screw manufactured from homogenized WE43 alloy.

With regard to the prospects for the implementation of the described processing approach for the use of the WE43 alloy in clinical practice, it can be stated that the loss of

integrity and the performance attributes of prospective implants may be alleviated by MAD processing. We believe that MAD treatment will reduce the risk of implant failures during the early postoperative period. It will also ensure a longer period of stable functioning of an implant, promoting its colonization with osteogenic cells and enabling the completion of osteosynthesis for bone reconstruction. We should also note that the growth of crystals that inhibit cell adhesion on the alloy surface can be inhibited (at least in the early stages of implantation, which is especially important for cell growth) by applying biodegradable coatings. Promising candidates for this role are materials based on calcium phosphate cements [33,34]. Not only are such coatings able to inhibit the degradation of magnesium at the early stages of implantation (and, therefore, to reduce the undesirable growth of crystals and the rate of hydrogen release), but they may also boost the biocompatibility of the finished products. Furthermore, it was previously shown that such coatings have good biocompatibility, do not have a negative effect on bone regeneration and exhibit additional antibacterial activity [35–37]. All that offers indisputable benefits when using the medical devices based on these coated alloys in orthopedics, including orthopedic oncology.

5. Conclusions

Through this study, we found that the treatment of the WE43 alloy by multiaxial deformation provides a change in its microstructure and grain size, leading to a desirable decrease in the rate of biodegradation in FBS and the complete cell growth medium based on DMEM. This results in a reduction in the rate of accumulation of biodegradation products in the immersion medium and, most importantly, a smooth decrease in the CT volume and mass loss of the prospective implant. A further result of MAD treatment is that it helps in reducing the level of alkalization of the cell growth medium. This leads to an increase in the viability of MMSCs during the first days of incubation, further stimulating the colonization by the osteogenic stromal cells of the alloy surface. In general, the process of biocorrosion of the WE43 alloy after MAD was characterized by smoother dynamics than of the alloy in the initial condition. This promises a greater stability of a medical device against biocorrosion after its intraosseous implantation, thus enabling a more efficient osteosynthesis. Ideally, this will make obsolete a need for repeat surgery to remove the device. The studies carried out have shown the prospects for the application of mechanical processing methods of traditional alloys to optimize the properties of developed medical devices for orthopedics. We expect that future research will yield additional information on the properties of implants based on the modified WE43 alloy *in vivo*, which will bring magnesium alloys closer to applications in medicine in general and in orthopedics, surgery, and oncology in particular.

Author Contributions: Conceptualization: N.A. and N.M.; methodology: M.K. and M.G.; software: N.A., N.M., K.N., O.R. and G.R.; validation: A.M., A.K. and B.S.; formal analysis: S.D. and Y.E.; investigation: N.A., N.M., K.N., O.R., M.G. and G.R.; resources: G.S., A.M., A.K., M.G. and M.K.; data curation: S.D., B.S. and Y.E.; writing—original draft preparation: N.A. and N.M.; writing—review and editing: N.A., N.M. and Y.E.; visualization: M.K.; supervision: S.D., M.K. and Y.E.; project administration: N.A. and A.M.; funding acquisition: N.A. All authors have read and agreed to the published version of the manuscript.

Funding: This work was supported by the Ministry of Science and Higher Education of the Russian Federation (Agreement No. 075-15-2021-965, #13.2251.21.0030).

Institutional Review Board Statement: The cell test protocols were evaluated and approved by the Local Ethics Committee of the “N.N. Blokhin National Medical Research Center of Oncology” of the Ministry of Health of the Russian Federation (protocol code 10/660, 14 October 2021).

Informed Consent Statement: No humans were involved in studies.

Data Availability Statement: All the data required to reproduce these experiments are present in the article.

Acknowledgments: The authors are grateful to G. Gerstein who supplied the WE43 castings used in this work, N. Yu. Yurchenko who carried out the multiaxial deformation processing and E.A. Akhmatova who helped with micro-CT data analysis.

Conflicts of Interest: The authors declare no conflict of interest.

References

1. Lopez, J.; Siegel, N.; Reategui, A.; Faateh, M.; Manson, P.N.; Redett, R.J. Absorbable Fixation Devices for Pediatric Craniomaxillo-facial Trauma: A Systematic Review of the Literature. *Plast. Reconstr. Surg.* **2019**, *144*, 685–692. [[CrossRef](#)] [[PubMed](#)]
2. Fonseca, A.C.; Serra, A.C.; Coelho, J.F.J. Bioabsorbable polymers in cancer therapy: Latest developments. *EPMA J.* **2015**, *6*, 1–18. [[CrossRef](#)]
3. Sheikh, Z.; Najeeb, S.; Khurshid, Z.; Verma, V.; Rashid, H.; Glogauer, M. Biodegradable Materials for Bone Repair and Tissue Engineering Applications. *Materials* **2015**, *8*, 5744–5794. [[CrossRef](#)] [[PubMed](#)]
4. Kanno, T.; Sukegaw, S.; Furuki, Y.; Nariai, Y.; Sekin, J. Overview of innovative advances in bioresorbable plate systems for oral and maxillofacial surgery. *Jpn. Dent. Sci. Rev.* **2018**, *54*, 127–138. [[CrossRef](#)] [[PubMed](#)]
5. Agarwal, S.; Gupta, A.; Grevious, M.; Reid, R.R. Use of resorbable implants for mandibular fixation: A systematic review. *J. Craniofac. Surg.* **2009**, *20*, 331–339. [[CrossRef](#)]
6. On, S.W.; Cho, S.W.; Byun, S.H.; Yang, B.E. Bioabsorbable Osteofixation Materials for Maxillofacial Bone Surgery: A Review on Polymers and Magnesium-Based Materials. *Biomedicines* **2020**, *8*, 300. [[CrossRef](#)] [[PubMed](#)]
7. Gareb, B.; van Bakelen, N.B.; Buijs, G.J.; Jansma, J.; de Visscher, J.G.A.M.; Hoppenreijts, T.J.M.; Bergsma, J.E.; van Minnen, B.; Stegenga, B.; Bos, R.R.M. Comparison of the long-term clinical performance of a biodegradable and a titanium fixation system in maxillofacial surgery: A multicenter randomized controlled trial. *PLoS ONE* **2017**, *12*, e0177152. [[CrossRef](#)] [[PubMed](#)]
8. Gareb, B.; van Bakelen, N.B.; Dijkstra, P.U.; Vissink, A.; Bos, R.R.M.; van Minnen, B. Biodegradable versus titanium osteosynthesis in maxillofacial traumatology: A systematic review with meta-analysis and trial sequential analysis. *Int. J. Oral Maxillofac. Surg.* **2020**, *49*, 914–931. [[CrossRef](#)] [[PubMed](#)]
9. Ma, J.; Zhao, N.; Betts, L.; Zhu, D. Bio-Adaption between Magnesium Alloy Stent and the Blood Vessel: A Review. *J. Mater. Sci. Technol.* **2016**, *32*, 815–826. [[CrossRef](#)] [[PubMed](#)]
10. Pang, T.Y.; Kwok, J.S.; Nguyen, C.T.; Fox, K. Evaluating magnesium alloy WE43 for bioresorbable coronary stent applications. *MRS Adv.* **2021**, *6*, 54–60. [[CrossRef](#)]
11. Oshibe, N.; Marukawa, E.; Yoda, T.; Harada, H. Degradation and interaction with bone of magnesium alloy WE43 implants: A long-term follow-up in vivo rat tibia study. *J. Biomater. Appl.* **2019**, *33*, 1157–1167. [[CrossRef](#)] [[PubMed](#)]
12. Dobatkin, S.; Martynenko, N.; Anisimova, N.; Kiselevskiy, M.; Prosvirnin, D.; Terentiev, V.; Yurchenko, N.; Salishchev, G.; Estrin, Y. Mechanical Properties, Biodegradation, and Biocompatibility of Ultrafine Grained Magnesium Alloy WE43. *Materials* **2019**, *12*, 3627. [[CrossRef](#)] [[PubMed](#)]
13. Martynenko, N.; Lukyanova, E.; Anisimova, N.; Kiselevskiy, M.; Serebryany, V.; Yurchenko, N.; Raab, G.; Birbilis, N.; Salishchev, G.; Dobatkin, S.; et al. Improving the property profile of a bioresorbable Mg-Y-Nd-Zr alloy by deformation treatments. *Materialia* **2020**, *13*, 100841. [[CrossRef](#)]
14. Rodríguez-Hernández, C.O.; Torres-García, S.E.; Olvera-Sandoval, C.; Ramírez-Castillo, F.Y.; Muro, A.L.; Avelar-Gonzalez, F.J.; Guerrero-Barrera, A.L. Cell culture: History, development and prospects. *Int. J. Curr. Res. Aca. Rev.* **2014**, *2*, 188–200.
15. Johnson, I.; Liu, H. A study on factors affecting the degradation of magnesium and a magnesium-yttrium alloy for biomedical applications. *PLoS ONE* **2013**, *8*, e65603. [[CrossRef](#)] [[PubMed](#)]
16. Janning, C.; Willbold, E.; Vogt, C.; Nellesen, J.; Meyer-Lindenberg, A.; Windhagen, H.; Thorey, F.; Witte, F. Magnesium hydroxide temporarily enhancing osteoblast activity and decreasing the osteoclast number in peri-implant bone remodelling. *Acta Biomater.* **2010**, *6*, 1861–1868. [[CrossRef](#)]
17. Cooper, S.L.; Peppas, N.A. *Biomaterials, Interfacial Phenomena and Applications.*; American Chemical Society: Washington, DC, USA, 1982.
18. Liu, C.-L.; Zhang, Y.; Zhang, C.-Y.; Wang, W.; Huang, W.-J.; Chu, P.K. Synergistic effect of chloride ion and albumin on the corrosion of pure magnesium. *Front. Mater. Sci.* **2014**, *8*, 244–255. [[CrossRef](#)]
19. Hedberg, Y.; Wang, X.; Hedberg, J.; Lundin, M.; Blomberg, E.; Odnevall Wallinder, I. Surface-protein interactions on different stainless steel grades: Effects of protein adsorption, surface changes and metal release. *J. Mater. Sci. Mater. Med.* **2013**, *24*, 1015–1033. [[CrossRef](#)] [[PubMed](#)]
20. Vidal, C.V.; Muñoz, A.I. Electrochemical characterisation of biomedical alloys for surgical implants in simulated body fluids. *Corros. Sci.* **2008**, *50*, 1954–1961. [[CrossRef](#)]
21. Bamford, C.; Cooper, S.L.; Tsurutta, T. *The Vroman Effect*; ASC Publications: Washington, DC, USA, 1992.
22. Heimke, G. *Osseo-Integrated Implants*; CRC Press: Boca Raton, FL, USA, 1990; Volume 2.
23. Esmaily, M.; Svensson, J.E.; Fajardo, S.; Birbilis, N.; Frankel, G.S.; Virtanen, S.; Arrabal, R.; Thomas, S.; Johansson, L.G. Fundamentals and advances in magnesium alloy corrosion. *Prog. Mater. Sci.* **2017**, *89*, 92–193. [[CrossRef](#)]

24. Parfenov, E.V.; Kulyasova, O.B.; Mukaeva, V.R.; Mingo, B.; Farrakhov, R.G.; Cherneikina, Y.V.; Yerokhin, A.; Zheng, Y.F.; Valiev, R.Z. Influence of ultra-fine grain structure on corrosion behaviour of biodegradable Mg-1Ca alloy. *Corros. Sci.* **2020**, *163*, 108303. [[CrossRef](#)]
25. Zhang, F.; Ma, A.; Jiang, J.; Xu, H.; Song, D.; Lu, F.; Nishida, Y. Enhanced biodegradation behavior of ultrafine-grained ZE41A magnesium alloy in Hank's solution. *Prog. Nat. Sci. Mater.* **2013**, *23*, 420–424. [[CrossRef](#)]
26. Jiang, J.; Zhang, F.; Ma, A.; Song, D.; Chen, J.; Liu, H.; Qiang, M. Biodegradable Behaviors of Ultrafine-Grained ZE41A Magnesium Alloy in DMEM Solution. *Metals* **2016**, *6*, 3. [[CrossRef](#)]
27. Hosaka, T.; Yoshihara, S.; Amanina, I.; MacDonald, B.J. Influence of Grain Refinement and Residual Stress on Corrosion Behavior of AZ31 Magnesium Alloy Processed by ECAP in RPMI-1640 Medium. *Procedia Eng.* **2017**, *184*, 432–441. [[CrossRef](#)]
28. Kavyani, M.; Ebrahimi, G.R.; Ezatpour, H.R.; Jahazi, M. Microstructure refinement, mechanical and biocorrosion properties of Mg–Zn–Ca–Mn alloy improved by a new severe plastic deformation process. *J. Magnes. Alloys* **2021**. [[CrossRef](#)]
29. Bairagi, D.; Mandal, S. A comprehensive review on biocompatible Mg-based alloys as temporary orthopaedic implants: Current status, challenges, and future prospects. *J. Magnes. Alloys* **2021**. [[CrossRef](#)]
30. Song, G.L.; Atrens, A. Corrosion mechanisms of magnesium alloys. *Adv. Eng. Mater.* **1999**, *1*, 11–33. [[CrossRef](#)]
31. Martynenko, N.S.; Anisimova, N.Y.; Temralieva, D.R.; Kiselevskiy, M.V.; Morozov, M.M.; Yusupov, V.S.; Dobatkin, S.V.; Estrin, Y.Z. Effect of rotary swaging and subsequent aging on the implant-relevant properties of magnesium alloy WE43. *J. Phys. Conf. Ser.* **2020**, *1688*, 012006. [[CrossRef](#)]
32. Barinov, S.M.; Komlev, V.S. Calcium Phosphate Bone Cements. *Inorg. Mater.* **2011**, *47*, 1470–1485. [[CrossRef](#)]
33. Bohner, M. Design of ceramic-based cements and putties for bone graft substitution. *Eur. Cells Mater.* **2010**, *20*, 3–10. [[CrossRef](#)] [[PubMed](#)]
34. Goldberg, M.A.; Krohicheva, P.A.; Fomin, A.S.; Khairutdinova, D.R.; Antonova, O.S.; Baikin, A.S.; Smirnov, V.V.; Fomina, A.A.; Leonov, A.V.; Mikheev, I.V.; et al. In situ magnesium calcium phosphate cements formation: From one pot powders precursors synthesis to in vitro investigations. *Bioact. Mater.* **2020**, *5*, 644–658. [[CrossRef](#)] [[PubMed](#)]
35. Mestres, G.; Ginebra, M.-P. Novel magnesium phosphate cements with high early strength and antibacterial properties. *Acta Biomater.* **2011**, *7*, 1853–1861. [[CrossRef](#)] [[PubMed](#)]
36. Ewald, A.; Kreczy, D.; Brückner, T.; Gbureck, U.; Bengel, M.; Hoess, A.; Nies, B.; Bator, J.; Klammert, U.; Fuchs, A. Development and Bone Regeneration Capacity of Premixed Magnesium Phosphate Cement Pastes. *Materials* **2019**, *12*, 2119. [[CrossRef](#)] [[PubMed](#)]
37. Fadeeva, I.V.; Lazoryak, B.I.; Davidova, G.A.; Murzakhanov, F.F.; Gabbasov, B.F.; Petrakova, N.V.; Fosca, M.; Barinov, S.M.; Vadalà, G.; Uskoković, V.; et al. Antibacterial and cell-friendly copper-substituted tricalcium phosphate ceramics for biomedical implant applications. *Mater. Sci. Eng. C* **2021**, *129*, 112410. [[CrossRef](#)] [[PubMed](#)]